Structure and reactivity of Au–Rh bimetallic clusters on titanate nanowires, nanotubes and TiO$_2$(1 1 0)

J. Kiss [a,b], L. Óvári [b], A. Oszkó [a], G. Pótári [a], M. Tóth [a], K. Baán [a], A. Erdóhelyi [a,b,*]

[a] Department of Physical Chemistry and Material Science, University of Szeged, Aradi vértanúk t. 1, H-6720 Szeged, Hungary
[b] Reaction Kinetics Research Laboratory, Institute of Nanochemistry and Catalysis, Chemical Research Center of Hungarian Academy of Sciences, P.O.B. 168, Aradi vértanúk t. 1, H-6701 Szeged, Hungary

A B S T R A C T

Au and Rh clusters, as well as Au–Rh bimetallic nanoparticles were prepared on titanate nanowires, nanotubes and on TiO$_2$(1 1 0). They were characterized by X-ray photoelectron spectroscopy (XPS), low energy ion scattering spectroscopy (LEIS) and Fourier transform infrared spectroscopy (FTIR). By performing careful LEIS experiments, it was found that for appropriate Au and Rh coverage, a thin Au layer almost completely covers the Rh nanoparticles, a Rh core–Au shell structure was detected. The formation of this structure was not affected by alkali (K) adatoms. LEIS and FTIR measurements disclosed that adsorbed CO at 300 K causes the segregation of Rh atoms to the surface of metal clusters in order to bind to CO. Upon CO adsorption on Rh/titanate nanostructures the IR stretching frequencies characteristic of the twin form were dominant, whereas bimetallic nanosystems featured a pronounced linear stretching vibration as well. In spite of this structure adsorbed CO is detectable during the ethanol adsorption on gold–rhodium bimetallic cluster and the ethanol decomposition rate is twice higher than on Au/TiO$_2$.

© 2011 Elsevier B.V. All rights reserved.

1. Introduction

Highly dispersed gold particles have increasingly gained attention in the catalytic community due to their unusual catalytic properties in a variety of oxidation and hydrogenation reactions [see e.g. Refs. [1–3] and references therein]. Supported bimetallic catalysts have been shown to exhibit superior catalytic performances when compared to their monometallic counterparts [4,5]. Depending on the nature of the second metal, different kinds of mechanisms were observed in the interactions with bimetals. Both ligand effects (i.e. an electronic factor due to the change in electron density) and ensemble effects (i.e. surface structure factor due to the positioning of different atom types) can contribute to synergetic effects often observed for bimetallic surface particles [6–8]. Enhanced dispersion and stability of gold nanoparticles on stoichiometric and reduced TiO$_2$(1 1 0) were observed in the presence of molybdenum [9]. It has also been observed that Rh significantly changed the morphology and topology of Au on TiO$_2$(1 1 0) surface [10,11]. STM and low energy ion scattering spectroscopy (LEIS) experiments revealed that at proper Au and Rh coverage the post-deposited Au completely and uniformly covers the Rh nanoparticles

(core–shell structure). In the case of the Au–Pd system the results show segregation of gold to the surface. Density functional theory calculation confirms that Au prefers to be at the edges of AuPd alloy particles under vacuum conditions [12]. The presence of Pt in the bimetallic Pt–Au clusters inhibits sintering, and the average size of the clusters after annealing decreases with increasing Pt content. Based on LEIS and STM experiments, performed on TiO$_2$(1 1 0), it was stated that the deposition of Au on Pt clusters results in the formation of bimetallic clusters due to the seeding of mobile Au atoms at existing Pt nuclei, but the deposition of Au on Pt does not produce core–shell structures with Au on top at small coverages [13]. Later on the formation of Pt core–Au shell structures was demonstrated at higher coverages (0.25–0.5 ML). Adsorption of CO on the Pt clusters covered by the gold capping layer promoted the diffusion of Pt atoms to the cluster surface in order to bind to CO [14].

In addition to the above findings it turned out that the nature of the support (i.e. Fe$_2$O$_3$(1 1 1), MgO(1 0 0), and CeO$_2$(1 1 1)) often plays a critical role in reactivity [4,5,12]. The observed vibrational frequency of CO adsorbed on the surface can be used to identify its specific binding sites and thus to elucidate the surface composition. Desorption of CO as a function of temperature provides similar information and supports the identification of binding sites on the surface. This approach has been successfully applied in the past to investigate Au–Pd alloy surfaces [15], Au–Pd particles supported on SiO$_2$ [16] and Al$_2$O$_3$ film [17], Au–Rh bilayers on supported powder TiO$_2$ [18] and on titanate nanowire and nanotubes [19,20].

* Corresponding author at: Department of Physical Chemistry and Material Science, University of Szeged, Aradi vértanúk t. 1, H-6720 Szeged, Hungary. Tel.: +36 62 343638; fax: +36 62 546482.
E-mail address: erdohely@chem.u-szeged.hu (A. Erdóhelyi).

Low energy ion scattering spectroscopy (LEIS), besides other surface sensitive techniques, was successfully applied in the characterization of bimetallic nanoclusters on $TiO_2(1\,1\,0)$ [9–11,13,14], because it has very high sensitivity in the topmost layer. In this paper we use this technique with XPS and FTIR methods to investigate the effect of potassium in the arrangement of Au–Rh clusters on $TiO_2(1\,1\,0)$ surface and on titanate nanowire and nanotubes supports.

One-dimensional nanostructures have been in the focus of the material science community for well more than a decade now [21]. Although carbon nanotubes may solve many challenges of materials engineering in the long run, at present their practical applicability appears to be limited by the lack of adequately selective synthesis technologies. On the other hand, inorganic nanostructures (e.g. metallic nanowires, oxides, sulfides, selenides, etc.) can be prepared in a rather controlled manner, and therefore their industrial-scale application is very close now.

Titanate nanotubes are also of great interest for catalytic applications, since their high cation exchange capacity provides the possibility of achieving a high metal dispersion [22]. In this regard, there are several demonstrated examples of successful utilization of titanate nanotubes as mesoporous catalyst supports for different nanoparticles. High-aspect-ratio TiO_2 and titanate nanoobjects are intensively studied at present because of their promising photoelectrical [23,24], biomedical [25], and hydrogen storage properties [26–28]. Gold-containing titania nanotubes were found to display higher activity in the photo-oxidation of acetaldehyde [29], the water–gas shift reaction [30], and CO oxidation [31] than the Degussa P-25 catalyst.

In this paper, we shall use the term "nanotube" for high-aspect-ratio objects with a hollow inner channel below 50 nm and "nanowire" for high-aspect-ratio objects without an inner void and a diameter below 200 nm.

The catalytic activity of titanate structures was tested in the ethanol decomposition. Catalytic conversion of bio-ethanol received considerable attention in the last decade [32–37] and the search for the most active, stable and selective catalyst has resulted in many heterogeneous catalytic systems.

Supported Rh is one of the best samples for these reactions, but only a few papers deal with the efficiency of supported Au. Idriss et al. [38] studied the oxidation of ethanol on Au/CeO_2, and the adsorption and desorption of it on Au/TiO_2 [39]. Guan and Hensen [40] recently examined the dehydrogenation of ethanol on Au nanoparticles deposited on various SiO_2 supports. A strong influence of the Au particle size was observed. It is noteworthy that, in the presence of oxygen, the intrinsic activity of Au/SiO_2 increased considerably. Lippits and Nieuwenhuys [41] investigated the conversion of ethanol into ethylene oxide on gold-based catalysts. It was found that when gold was added to the Al_2O_3 support the catalyst produced ethylene oxide which was not observed on the support alone. The presence of gold nanoparticles is necessary for the formation of ethylene oxide. Solymosi and co-workers [37] studied the ethanol decomposition on Au nanoparticles deposited on various oxides. The formation of hydrogen and the product distribution depended sensitively on the nature of the support. These samples catalyze mainly the dehydrogenation of ethanol, to produce hydrogen and acetaldehyde. The highest rate of hydrogen evolution was observed on Au/CeO_2.

2. Experimental

Titanate nanowires and nanotubes were prepared by hydrothermal conversion of anatase TiO_2 as described elsewhere [42,43]. Briefly, the nanostructures were prepared by mixing 2 g of anatase into 140 cm^3 10 M aqueous NaOH solution until a white suspension was obtained, aging the suspension in a closed, cylindrical,

Teflon-lined autoclave at 400 K for 1–72 h while rotating the whole autoclave intensively at 60 rpm around its short axis, and finally washing the product with deionized water and neutralizing with 0.1 M HCl acid solution to reach pH = 7; at this point, the slurry was filtered and the residue was dried in air at 353 K. Au, Rh and their coadsorbed layers with different compositions were produced by impregnating titania nanowires and nanotubes with the mixtures of calculated volumes of $HAuCl_4$ (Fluka) and $RhCl_3 \cdot 3H_2O$ (Johnson Matthey) solutions to yield 1 wt% metal content. In the bimetallic catalyst the Au/Rh atomic ratio was 1. The impregnated powders were dried in air at 383 K for 3 h, than oxidized at 573 K. The final pre-treatment was at 573 K in hydrogen atmosphere [18].

Titanate nanotubes are open ended hollow tubular objects measuring 7–10 nm in outer diameter and 50–170 nm in length. They feature a characteristic spiral cross section composed of 4–6 wall layers. The typical diameter of their inner channel is 5 nm. Titanate nanowire represents the thermodynamically most stable form of sodium trititanate under the applied alkaline hydrothermal conditions (note that the post-synthetic neutralization step converts the original $Na_2Ti_3O_7$ into its hydrogen form without affecting the nanowire morphology). Their diameter is 45–110 nm and their length is between 1.8 and 5 μm. The specific surface area of titanate nanotubes is rather large ($\sim$185 $m^2\,g^{-1}$) due to their readily accessible inner channel surface, whereas that of solid titanate nanowires is $\sim$20 $m^2\,g^{-1}$. The impurity level of produced nanocomposites was less than 1%. The foreign elements determined by XPS were K, Ca, Mg and Na remained from the preparation process.

The ultra high vacuum experiments were done in two separate chambers. One of them (1) was used to analyze the high area titanate samples, while measurements related to $TiO_2(1\,1\,0)$ were conducted in the other (2).

1. XP spectra were taken with a SPECS instrument equipped with a PHOIBOS 150 MCD 9 hemispherical analyzer. The analyzer was operated in the FAT mode with 20 eV pass energy. The Al K_α radiation ($h\nu$ = 1486.6 eV) of a dual anode X-ray gun was used as an excitation source. The gun was operated at the power of 150 W (12.5 kV, 12 mA). The energy step was 25 meV, electrons were collected for 100 ms in one channel. Typically five scans were summed to get a single high resolution spectrum. For binding energy reference the Ti $2p_{3/2}$ maximum (458.9 eV) was used. The same data were obtained when C 1s (adventitious carbon at 285.1 eV), or O 1s lattice oxygen (530.4 eV) was used as references. A sample preparation chamber was directly connected to the measuring chamber to avoid the contamination of samples between each step. For spectrum acquisition and evaluation both manufacturer's (SpecsLab2) and commercial (CasaXPS, Origin) software packages were used.

A SPECS IQE 12/38 ion source was used for generation of low-energy scattering (LEIS) spectra. He$^+$ ions of 800 eV kinetic energy were applied at a low ion flux equal to 0.03 μA/cm^2, which was necessary to avoid the sputtering of surface. The incident angles was 55° (with respect to surface normal), ions ejected along the surface normal were detected. The ion energies (LEIS) were measured by the same hemispherical energy analyzer as mentioned above.

2. Experiments related to the $TiO_2(1\,1\,0)$ single crystal were conducted in a separate UHV chamber. The crystal was a product of PI-KEM. Its temperature could be changed between 150 and 1000 K. The sample was cleaned at 1000 K, applying Ar$^+$ ion sputtering (2.5 μA, 1.5 keV, 10 min) and vacuum annealing (5 min) cycles. The final treatment was Ar$^+$ ion sputtering at 300 K (30 min). Metals were deposited from an e-beam evaporator of Oxford Applied Research. The chamber had facilities for Auger electron spectroscopy (AES), XPS and LEIS. Electrons as well as He$^+$ ions were detected by a Leybold EA 10/100 hemispherical analyzer. During LEIS measurements, the incident and detection angles were 50° (with respect to surface normal), and the scattering angle was 95°.

An Al K$_\alpha$ anode was used as an X-ray source, and the binding energy scale was referenced to the 4f$_{7/2}$ peak of a thick Au layer set to 83.8 eV.

IR studies were performed in a high vacuum system. The samples were pressed onto a Ta-mesh. The mesh was fixed to the bottom of a conventional UHV sample manipulator. It was resistively heated and the temperature of the sample was measured with a NiCr–Ni thermocouple spot welded directly to the mesh. IR spectra were recorded with a Genesis (Mattson) FTIR spectrometer. The whole optical path was purged by a Balston 75-62 FTIR purge generator.

DRIFT spectra were registered during the ethanol adsorption with Bio-Rad FTIR spectrometer with wave number accuracy of $\pm 4\,cm^{-1}$. The instrument was equipped with a diffuse reflectance attachment (Spectra-Tech) with BaF$_2$ windows. Typically 32 scans were registered. The catalysts were pretreated as mentioned above and the sample was cooled down to room temperature. Then ethanol was introduced into the cell by bubbling Ar gas through ethanol at 273 K while the sample was heated linearly with a heating rate of 10 K/min up to 573 K. The IR spectra were registered continuously.

The catalytic experiments were carried out in a fixed bed continuous flow reactor (8 mm o.d. quartz tube), which was heated externally. The dead volume of the reactor was filled with quartz beads. For catalytic studies small fragments (1–3 mm) of slightly compressed pellets were used. Typically 50 mg of catalysts was used. Ethanol was introduced into the reactor by bubbling the carrier gas (Ar 80 ml/min) through liquid ethanol cooled to 273 K. Analysis of the products and reactants was performed with a Chrompack 9001 gas chromatograph using Porapack QS column. The gases were detected simultaneously by TC and FI detectors.

3. Results and discussion

3.1. LEIS experiments obtained on a potassium containing TiO$_2$(1 1 0) surface

In our previous papers it was demonstrated that Rh core–Au shell clusters can be prepared on TiO$_2$(1 1 0) if Au is postdeposited by physical vapor deposition (PVD) on the oxide surface containing Rh clusters [10,11]. No separate Au clusters formed in the process at a substrate temperature of 500 K. The existing Rh clusters act as nucleation centers for gold atoms deposited subsequently. The high diffusion rate of Au atoms on the oxide during evaporation probably plays an important role in this process. Earlier [11] we demonstrated that the formation of core–shell Rh–Au particles did not depend on the state of reduction of the surface: it proceeded both on unreconstructed TiO$_2$(1 1 0) and also on the more reduced TiO$_2$(1 1 0) − (1 × 2).

The thermodynamic driving force that Au atoms tend to be outside within bimetallic clusters comes from the significantly lower surface free energy of Au compared to Rh [44]. When the reverse deposition sequence was applied, i.e. Rh was deposited on the Au/TiO$_2$(1 1 0) surface, a very efficient place exchange between Rh and Au atoms was observed by LEIS even at room temperature, moving Rh atoms into subsurface regions of bimetallic clusters and the cluster surface remained covered by gold [10]. This indicates that diffusion processes within small metal clusters are rather facile compared to bulk materials.

Considering the important role of alkali promoters in catalysis and that alkaline atoms/ions are typical constituents/impurities in titanate nanotubes and nanowires it seemed worth investigating whether the formation of core–shell Rh–Au clusters proceeds on a potassium containing TiO$_2$(1 1 0) surface as well.

The potassium overlayer was prepared by thermal segregation: annealing the cleaned sputtered surface at $T \geq 800\,K$ (5 min)
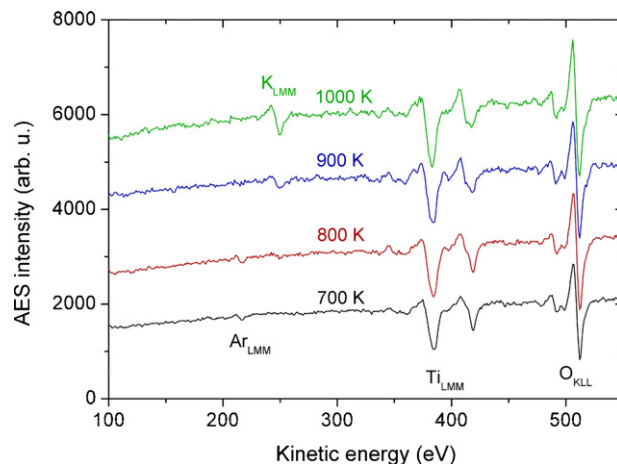

Fig. 1. Auger spectra obtained after annealing the TiO$_2$(1 1 0) surface – previously Ar$^+$ sputtered at 300 K – at higher temperatures in UHV for 5 min.

resulted in the appearance of potassium on the surface detected by AES and XPS. Generally, the potassium content of a TiO$_2$ crystal is exhausted by sputtering-annealing cycles within a few weeks, but with this sample the K coverage obtained by the 5 min annealing at 1000 K was stable during the period of these experiments (~2 month), characterized by a K/Ti AES ratio of 0.4 monitoring the K$_{LMM}$ (252 eV) and Ti$_{LMM}$ (387 eV) peaks (Fig. 1). Other typical impurities (Ca, Na) were not present on this surface.

The chemical state of the potassium containing TiO$_2$(1 1 0) surface obtained after 5 min annealing at 1000 K was analyzed by XPS. The Ti 2p$_{3/2}$ peak was observed at 458.7 eV (not shown), which is typical for Ti^{4+} ions in the titania surface. Apparently no dramatic shifts or increased reduction was found due to the presence of potassium. The Ti 2p feature, collected at a detection angle of 16° (with respect to surface normal) contained a small contribution of Ti^{3+} sites, with an area of ca. 6.5% compared to the area of the Ti^{4+} doublet. This is rather typical for a used TiO$_2$(1 1 0) crystal, already colored dark blue. The peak positions were identical, when the Ti 2p region was monitored at a grazing (71°) detection angle, resulting in a smaller information depth. However, the extent of reduction was somewhat larger, resulting in a Ti^{3+} component with an area of ca 10% of the area corresponding to the Ti^{4+} component. Evidently this difference is a clear sign that more defect sites exist in the top surface region. The K 2p$_{3/2}$ peak (not shown) was found at 294.0 eV indicating that K atoms at the surface are partially ionized [45].

The possible formation of core–shell Rh–Au clusters on the potassium covered TiO$_2$(1 1 0) surface was investigated by LEIS. The scattering angle in that chamber was relatively small (95°), which is advantageous for the sensitivity, but results in a lower resolution. Consequently, the LEIS contributions of K and Ti are merged into one peak, because of the similar masses of these elements. First, 0.5 ML of Rh was evaporated on K/TiO$_2$(1 1 0) at a substrate temperature of 330 K. Annealing to 500 K did not cause any appreciable change monitored by LEIS. Gold was subsequently deposited at 500 K and the changes in the LEIS intensities as a function of Au coverage are shown in Fig. 2.

The Rh peak decreased steeply with increasing amounts of gold, while the intensities of the O peak and of the peak corresponding to K and Ti were only mildly attenuated. Evidently Au atoms evaporated on the sample nucleated on existing Rh clusters. If only Au atoms landed on top of Rh clusters during evaporation had been stabilized on top of Rh, than the complete disappearance of Rh signal would have occurred approximately at the coverage of 1 ML or even above, considering the curvature of the clusters. However, the Rh signal in our measurements decreased to zero at a much
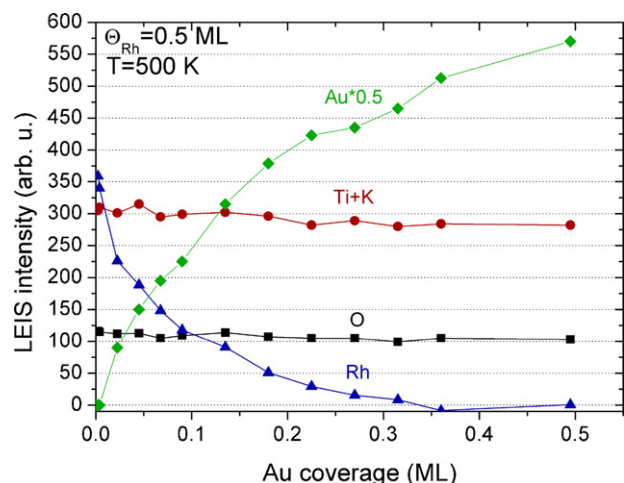
Fig. 2. Changes in LEIS intensities due to Au deposition at 500 K on the K/TiO$_2$(1 1 0) surface precovered with 0.5 ML of Rh.

smaller coverage (0.35 ML). This indicates that a major fraction of gold atoms – impinged on the free oxide surface during evaporation – migrated to Rh clusters and was stabilized there, similarly as it was demonstrated for the potassium-free TiO$_2$(1 1 0) surface in our previous papers [10,11]. At a substrate temperature of 450 K analogue results were obtained, but the process was not investigated at even lower *T* values in order to avoid the effect of background CO on LEIS intensities.

3.2. Results obtained on titanate nanowires and nanotubes

The surface composition of Au–Rh clusters on titanate nanocomposite was also investigated by LEIS. As was observed in the case of TiO$_2$(1 1 0) substrate, with increasing gold content the Rh LEIS intensity decreased dramatically. The most pregnant feature was observed in the 0.5% Au + 0.5% Rh case. On the monometallic systems the gold and rhodium He$^+$ scattering signals appeared at 753 and 707 eV, respectively. On bimetallic nanocomposite, however, only the gold signal showed up (Fig. 3) [20]. The rhodium peak was just a bit higher than the noise level. It is very interesting that while the gold content is less (0.5%) in bimetallic system, the LEIS intensity of Au is higher than in the monometallic (1%) case.

On the monometallic Rh/TiO$_2$ nanowire the dominant XP peak for Rh 3d$_{5/2}$ appeared at 307.1 eV after reduction at 573 K (not shown). The tailing at the higher binding energy side of this emission may consist of the original asymmetry and trace of foreign element (Mg KLL Auger peak) that remained from the preparation process. A careful deconvolution revealed some emission at 309.3 eV, presumably due to more dispersed nanoparticles. Very similar rhodium XP spectra were recorded on titanate nanotubes. In the case of the 1% Au/TiO$_2$ nanowire two peaks were observed on the reduced sample for Au 4f$_{7/2}$ at 83.7 eV (metallic state) and 85.6 eV. The emission at 85.6 eV cannot be attributed to a kind of higher oxidation state, because it developed after hydrogen treatment at 573 K. We may attribute this feature to gold atoms in very small sized nanoparticles ("final-state" effect) [19,20]. Under drastic conditions of an oxygen plasma gold oxide formation was observed; the Au 4f$_{7/2}$ was observed above 85 eV [46]. We found that the feature at 85.6 eV appeared only after reduction and not after oxidation so we exclude the oxidized Au formation.

The XP spectra of the bimetallic Au + Rh layer supported on titania nanowires are shown in Fig. 4. Surprisingly, the emission for the higher energy peak of Au 4f$_{7/2}$ at 85.6 eV corresponding to the atomically dispersed state is very small in the presence of Rh (Fig. 4A), and at the same time the emission for Rh 3d$_{5/2}$ at around 309.3 eV

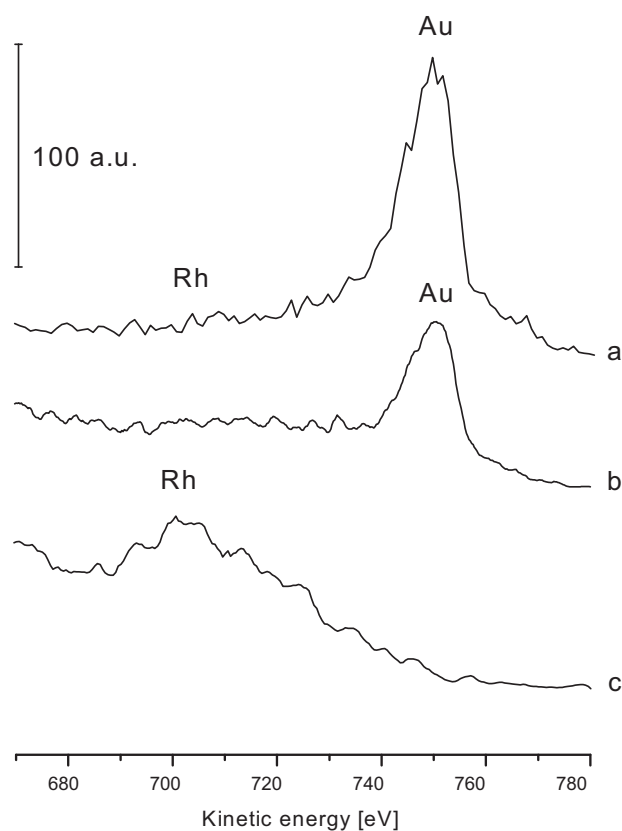### LEIS spectra taken on titanate nanowire

Fig. 3. LEIS spectra of 1% Au/TiO$_2$ (b), 1% Rh/TiO$_2$ nanowire (c), 0.5% Au + 0.5% Rh/TiO$_2$ nanowire (a) [20].

also diminished. The adsorption of CO at 300 K did not alter the position of gold emissions. The Rh XPS feature at 308.9–309.3 eV appeared or intensified a little bit after 60 min CO adsorption may be due to the appearance of more dispersed particles (Fig. 4B). The CO pressure was 1.3 mbar in the preparation chamber.

The morphology of Au, Rh and Au + Rh supported on TiO$_2$ nanowires and nanotubes was investigated by FTIR, employing adsorbed CO as a probe molecule sensitive to the local surface structure. Adsorbed CO exhibits at least three different stretching frequencies belonging to certain adsorption sites of Rh on oxide supports [46]. The band at 2070–2030 cm^{-1} is due to CO adsorbed linearly to Rh^0 (depending on the coverage), the band at ~1855 cm^{-1} represents the bridge bonded CO (Rh$_2$–CO), and the feature at ~2100 cm^{-1} and at ~2020 cm^{-1} corresponds to the symmetric and asymmetric stretchings of Rh$^+$(CO)$_2$ (twin CO). These latter IR signals were detected when the crystallite size was very small [47]. CO adsorption on gold supported on titania nanostructure was not observed. On monometallic Rh supported on nanowire practically the twin form was present (2027 and 2097 cm^{-1}), the linear form between these two peaks was much smaller and the bridge form was hardly observable (Fig. 5A). On nanotubes the linearly adsorbed CO features showed up at 2075 cm^{-1} between the peaks at 2100 and 2036 cm^{-1} (twin form) (not shown). From these IR studies we may conclude that a significant part of Rh exists in small particle sizes on both nanowires and tubes.

It is plausible if the gold completely and uniformly covers the Rh nanoparticles (core–shell structure) adsorbed CO could not be detected by FTIR. However, the situation is that relatively strong CO bands appeared at 300 K at a pressure of 1.3 mbar. In the presence
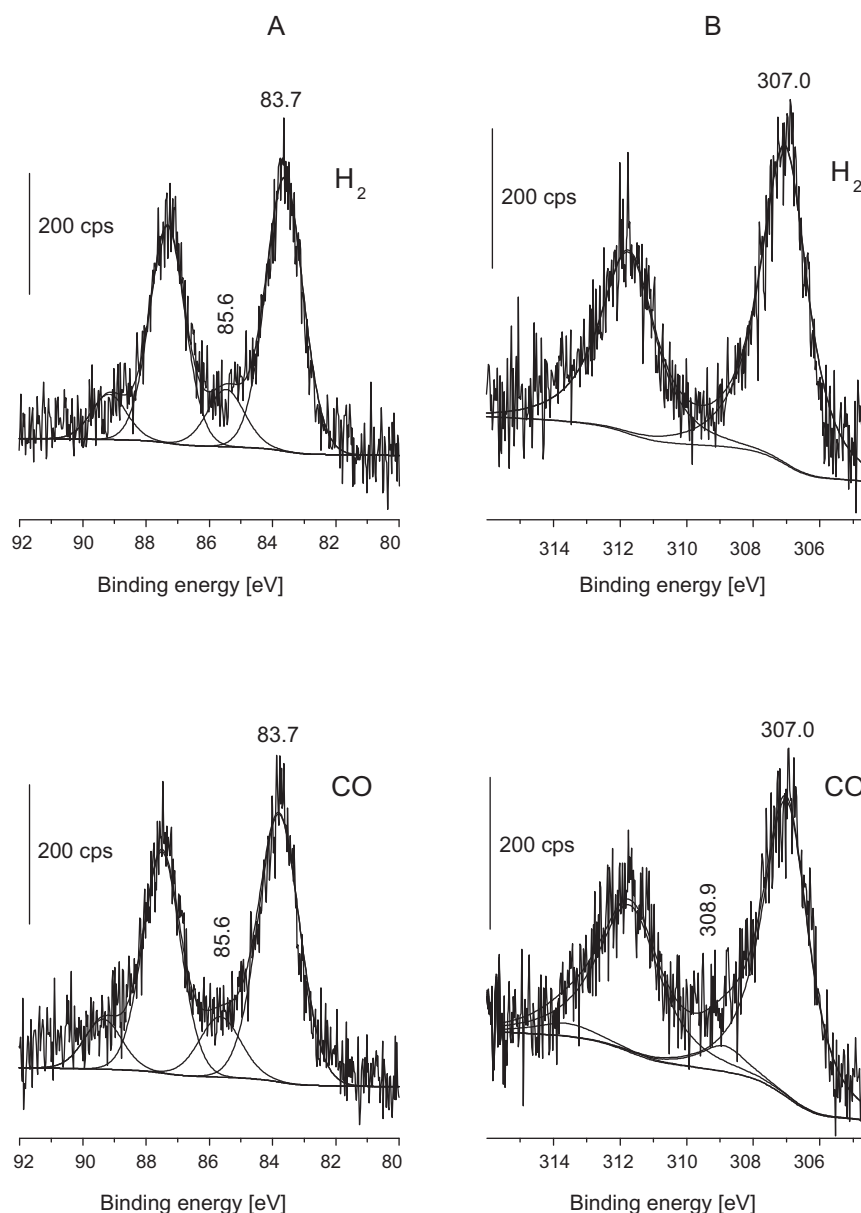
Fig. 4. XP spectra of Au 4f (A) and Rh 3d (B) of 0.5% Au + 0.5% Rh/TiO$_2$ nanowire before and after CO treatment. The CO pressure was 1.3 mbar.

of gold, the peak corresponding to the linear form became stronger at 2070–2071 cm^{-1} and the twin CO stretching frequencies decreased (Fig. 5B). Seemingly there is a contradiction between the results of LEIS and CO adsorption infrared experiments. On the topmost layer there are no Rh atoms (Fig. 3), but adsorbed CO was detected by FTIR on this surface (Fig. 5B). This discrepancy can be explained by a CO induced surface reconstruction. The adsorption of CO on Au–Rh clusters may promote the diffusion of Rh to the surface of the cluster. Similar phenomena was observed recently in the case of bimetallic Pt–Au clusters on TiO$_2$(1 1 0) [14]. The same effect was also observed on Pd–Au bimetallic model catalysts, synthesized either as thin films on Mo(1 1 0) or as nanoparticles on TiO$_2$ thin film in CO oxidation at elevated (8–16 Torr) CO pressures [48]. Pd preferentially segregates to the surface to form contiguous Pd sites and CO oxidation reactivity is regained. The differences obtained on FTIR spectra between monometallic Rh and bimetallic Au–Rh nanoclusters on titanate nanowire are not surprising. The presence of the core–shell composites and the separate highly dispersed gold clusters may significantly affect the morphology

and electronic structure of Rh nanoparticles therefore the bonding modes of CO adsorbed on Rh sites. The observed FTIR feature may be related to the XPS result detected after CO adsorption. The morphology and crystallite size of segregated Rh could be different in surrounding of Au–Rh core–shell and in the inside of the core–shell structure.

In order to get closer to the understanding of CO-induced morphological changes some low energy ion scattering measurements (LEIS) were carried out before and after CO adsorption on Au–Rh bimetallic cluster supported on titanate nanotubes. In these experiments two compositions were used: 0.25%Au + 0.75%Rh/TiO$_2$ and 0.5%Au + 0.5%Rh%/TiO$_2$ nanotubes. The results are represented in Fig. 6. In order to avoid or minimize the sputtering effect of the He ions we applied relatively low ion flux (0.03 μA/cm^2). At the lower gold content rhodium scattering appeared at 707 eV after hydrogen treatment at 573 K. After CO adsorption at 300 K its intensity increased by about 20% (Fig. 6A). The effect of adsorbed CO was more pronounced in the 0.5% Au + 0.5% Rh case. Practically no or very small Rh scattering signal was detected indicating that the
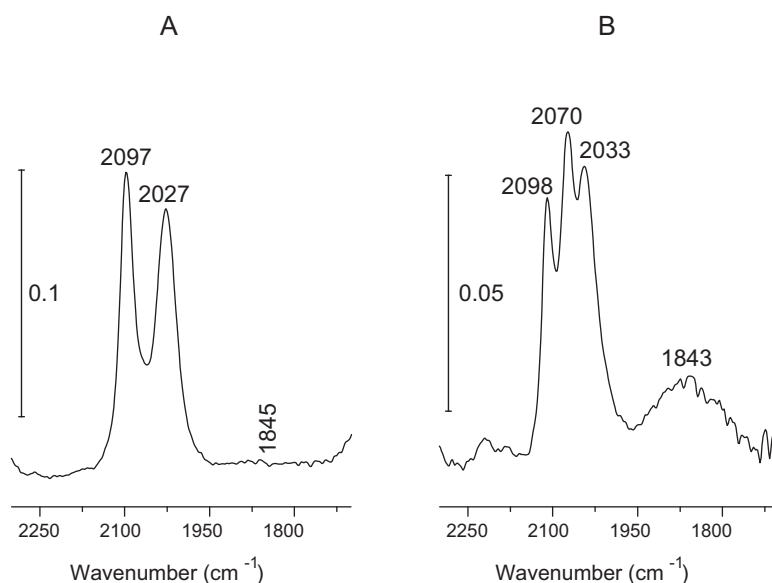
A B

Fig. 5. FTIR spectra of adsorbed CO at 300 K: (A) 1% Rh/TiO$_2$ nanowire and (B) 0.5% Au + 0.5% Rh/TiO$_2$ nanowire. The CO pressure was 1.3 mbar.

gold covered the rhodium particles (Fig. 6B), similarly the nanowire case (Fig. 3). When CO was added to the bimetallic composite, the rhodium ion scattering signal showed up. These experimental data strongly support the above mentioned phenomena, namely that CO induces a reconstruction of the surface. Rh preferentially segregates to the surface to form Rh–CO bond.

This process may imply the migration of Rh or Au atoms within the clusters or on the surface of the clusters. Considering that Au–Au and Au–Rh bonds are weaker than Rh–Rh bonds, it may appear more probable that the movement of Au atoms is more important

Fig. 6. LEIS spectra of 0.25% Au + 0.75% Rh/TiO$_2$ nanotube (A), 0.5% Au + 0.5% Rh/TiO$_2$ nanotube (B) before and after CO adsorption at 300 K. The CO pressure was 1.3 mbar.

(the shell "opens"), while Rh atoms move less. The influence of CO gas in this possible process is an important question. Though the Au–CO interaction is rather weak compared to Rh–CO bond, in the relatively high CO pressure applied, the CO coverage on the Au capping layer is probably significant. The adsorbed CO layer presumably decreases the metal-metal bonds both for Au and Rh, leading to an increased diffusion rate. It is also possible that CO, adsorbed in some hollow site of the Au layer can form some kind of bond with subsurface Rh atoms and this interaction promotes the displacement of Au atoms and the segregation of Rh.

Another possible scenario is that there is a continuous thermal fluctuation of metal atoms within the bimetallic clusters independent of the presence of CO, and for short periods Rh atoms can be found on the cluster surface, which are subsequently trapped by CO. The existence of this fluctuation may be possible, since significant movement of metal atoms within small clusters at room temperature was observed in several cases [10,49,50] characterized by diffusion coefficients many orders of magnitude higher than the corresponding bulk values. Anyhow, further studies are needed to understand in detail the CO induced restructuring of Rh–Au clusters.

3.3. Ethanol adsorption on titanate nanowire supported catalysts

During ethanol adsorption at room temperature predominantly the carbon–carbon bond dissociates and the carbon–oxygen bond is preserved leading to adsorbed CO but no to adsorbed atomic O on Rh(1 1 1) [51] surfaces. In addition to CO, also significant amounts of methylidyne and ethylidyne species are formed on Rh(1 1 1), the latter presumably via a reforming reaction. Gong and Mullins [52] reported that on Au(1 1 1) ethanol adsorbs only weakly and desorbs molecularly. Ethanol adsorption has been extensively studied by IR spectroscopy over TiO$_2$ and TiO$_2$ supported metals [53,54] among others on Rh/TiO$_2$ [55] and Au/TiO$_2$ [39], too.

Fig. 7 shows the DRIFT spectra of ethanol adsorbed on 1% Au/TiO$_2$, 0.5% Au + 0.5% Rh/TiO$_2$ and 1% Rh/TiO$_2$ catalyst at different temperatures. Similar spectra were registered in all cases excepting the CO region. These results support that these species adsorbed on the nanowire. At 300 K absorption bands were observed at 2974, 2929 and 2875 cm^{-1} in the C–H stretching region. In the low frequency range absorption bands were detected at 1448–1450
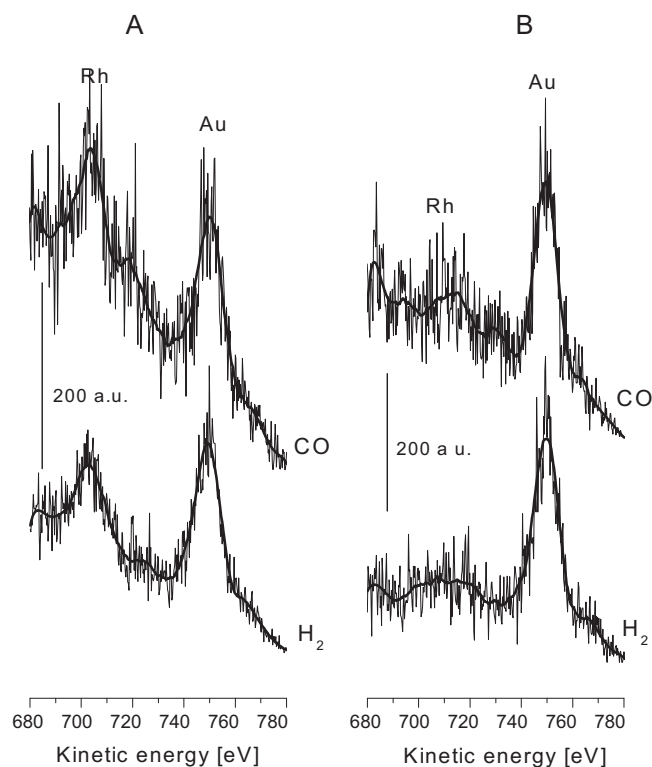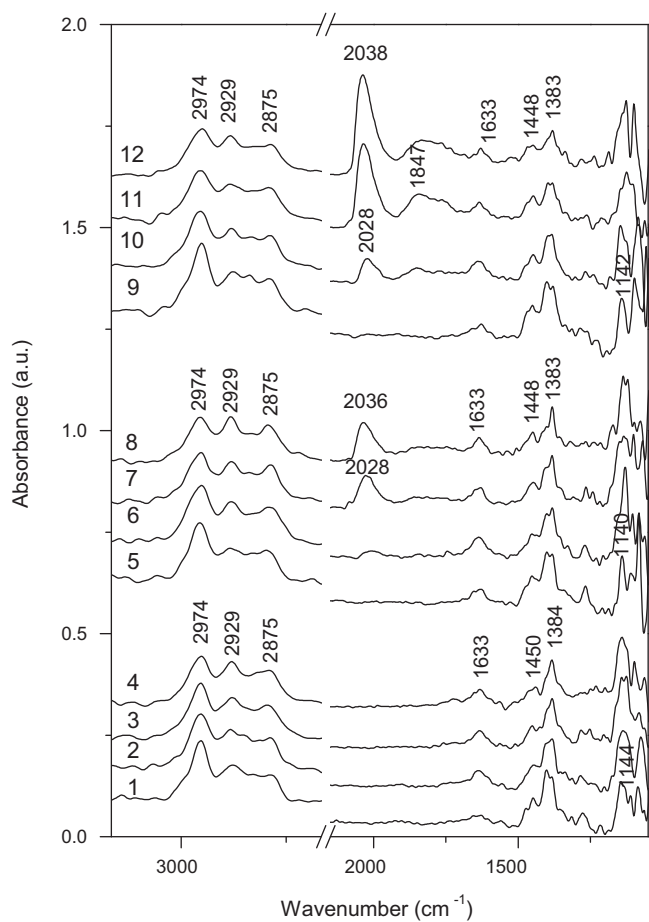
Fig. 7. Infrared spectra of ethanol adsorbed at room temperature (1, 5, 9), at 373 (2, 6, 10), 423 (3, 7, 11), 473 K (4, 8, 12) on 1% Au/TiO$_2$ nanowire (1–4), 0.5% Au + 0.5% Rh/TiO$_2$ nanowire (5–8), and 1% Rh/TiO$_2$ nanowire (9–12).

and 1383–1384 cm^{-1}, both could be assigned as δCH$_3$ vibrations of ethanol. The bands observed at 1140–1144, 1124–1121, 1069–1074, 1045–1047 cm^{-1} could be attributed to νC–O and C–C vibrations of monodentate and bidentate ethoxide species [39,55]. The intensities of these bands decreased as the temperature increased but dramatic changes were not detected.

Here we focus on the CO region where significant differences were observed. On Au/TiO2 we did not observe any absorbance between 2100 and 1800 cm^{-1} during ethanol adsorption as was found after CO adsorption [20]. When the Rh/TiO$_2$ was treated with ethanol above 373 K new peaks were detected at 2028 and 1847 cm^{-1}. The intensities of these bands increased with increasing the temperature and the peak observed at 2028 cm^{-1} at room temperature shifted to higher wave numbers. The absorbance at 1847 cm^{-1} could be attributed to bridge bonded CO on Rh sites [47,55]. The feature of the adsorbed CO detected at 2028–2038 cm^{-1} is significantly differing from that depicted in Fig. 5. This discrepancy could be explained by the Rh carbonyl hydride formation (H–Rh–CO) [55,56].

When 0.5% Au + 0.5% Rh/TiO$_2$ was the catalyst to our surprise nearly the same spectra were observed as in the case of 1% Rh/TiO$_2$ only the intensities of the bands were weaker; at 373 K a small peak was detected at about 2028 cm^{-1} attributed to adsorbed CO.

According to the XPS results binding energies of Rh and Au did not alter during the ethanol adsorption even at higher temperature. The C 1s spectra showed formation of different carbon oxygen containing species ($\sim$ 289 and 286.3 eV).
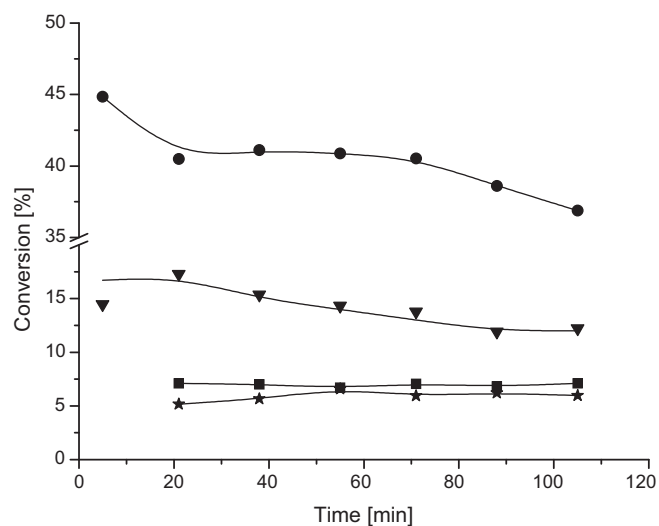

Fig. 8. The conversion of ethanol in the decomposition reaction at 603 K on TiO$_2$ nanowire (■), 1% Au/TiO$_2$ nanowire (★), 0.5% Au + 0.5% Rh/TiO$_2$ nanowire (▼) and 1% Rh/TiO$_2$ nanowire (●).

3.4. Ethanol decomposition on titanate nanowire supported catalysts

The ethanol decomposition was investigated at 603 K on Au, Rh and Au–Rh supported on titanate nanowire. The main products were in all cases carbon monoxide, methane, hydrogen, acetaldehyde, but ethylene, diethyl ether and acetic acid were also detectable. The ethanol conversion on titanate nanowire was slightly higher (7.1%) than on Au/TiO$_2$ (6%) (Fig. 8) but in the latter case the acetaldehyde selectivity was more than twice higher (37%) than on the clean support. Earlier it was also found that the supported Au particles catalyze mainly the dehydrogenation of ethanol, to produce hydrogen and acetaldehyde [37]. When the catalyst contains Rh the conversion significantly increased; on 0.5% Au-0.5% Rh/TiO$_2$ it was 12.2% and on Rh/TiO$_2$ the conversion was about five times higher (36.9%) than on Au/TiO$_2$ (Fig. 8). The product distributions were similar on both samples, mainly CO was formed the acetaldehyde selectivity was only 4–6%. It should be noted that in these cases the ethanol consumption decreased in time while in other cases it was stable.

From DRIFT and catalytic measurements we conclude that gold does not block entirely the adsorption and the active sites of Rh in a core–shell structure. The ethanol or the CO produced in the ethanol decomposition may also induce the segregation of Rh and the 0.5% Au + 0.5% Rh supported on titanate nanowire acts as an effective catalyst in ethanol decomposition.

4. Conclusions

1. Au and Rh clusters, as well as Au–Rh bimetallic nanoparticles were prepared on titanate nanowires, nanotubes and on TiO$_2$(1 1 0). The samples were characterized by X-ray photoelectron spectroscopy (XPS), low energy ion scattering spectroscopy (LEIS) and Fourier transform infrared spectroscopy (FTIR). By performing careful LEIS experiments, it was found that, for appropriate Au and Rh coverage, the Au almost completely covers the Rh nanoparticles. Rh core–Au shell structure was detected. The formation of this structure was not affected by alkali (K) adatoms. LEIS and FTIR showed that adsorbed CO at 300 K causes the segregation of Rh to the surface in order to bind to CO.

2. Rh supported on titanate nanowire exhibit a high catalytic activity in ethanol decomposition. In bimetallic form it preserves its activity because the ethanol similarly to CO may also induce the segregation of Rh from the Au-shell Rh-core structure.

Acknowledgements

References

[1] G.C. Bond, C. Louis, D.T. Thompson, Catalysis by Gold, Imperial College Press, London, 2006.
[2] M. Haruta, Gold Bull. 37 (2004) 27.
[3] G. Hutchings, J. Chem. Commun. (2008) 1148.
[4] J.A. Rodriguez, Surf. Sci. Rep. 24 (1996) 23 (and references therein).
[5] J.G. Chen, C.A. Menning, M.B. Zeller, Surf. Sci. Rep. 63 (2008) 201 (and references therein).
[6] A. Gross, Top. Catal. 37 (2006) 29.
[7] L. Guczi, Catal. Today 101 (2005) 53 (and references therein).
[8] L. Guczi, G. Boskovic, E. Kiss, Catal. Rev. Sci. Eng. 52 (2010) 133 (and references therein).
[9] L. Bugyi, A. Berkó, L. Óvári, A.M. Kiss, J. Kiss, Surf. Sci. 602 (2008) 1650.
[10] L. Óvári, L. Bugyi, Zs. Majzik, A. Berkó, J. Kiss, J. Phys. Chem. C 112 (2008) 1811.
[11] L. Óvári, A. Berkó, N. Balázs, Zs. Majzik, J. Kiss, Langmuir 26 (2010) 2167.
[12] H.L. Abbott, A. Aumer, Y. Lei, C. Asokan, R.J. Meyer, M. Sterrer, S. Shaikhutdinov, H.-J. Freund, J. Phys. Chem. 114 (2010) 17099.
[13] J.B. Park, S.F. Conner, D.A. Chen, J. Phys. Chem. C 63 (2008) 5490.
[14] S.A. Tenny, J.S. Ratliff, C.C. Roberts, W. He, S.C. Ammal, A. Heyden, D.A. Chen, J. Phys. Chem. C 114 (2010) 21652.
[15] Z. Li, F. Gao, O. Furlong, W.T. Tyose, Surf. Sci. 64 (2010) 136.
[16] K. Luo, T. Wei, C.W. Yi, S. Axnada, D.W. Goodman, J. Phys. Chem. B 109 (2005) 23517.
[17] D.R. Rainer, C. Xu, P.M. Holmblad, D.W. Goodman, J. Vac. Sci. Technol. 15 (1997) 1653.
[18] J. Kiss, R. Németh, Á. Koós, J. Raskó, J. Nanosci. Nanotechnol. 9 (2009) 3828.
[19] A. Oszkó, G. Pótari, A. Erdőhelyi, A. Kukovecz, Z. Kónya, I. Kiricsi, J. Kiss, Vacuum 85 (2011) 114.
[20] A. Kukovecz, G. Pótari, A. Oszkó, Z. Kónya, A. Erdőhelyi, J. Kiss, Surf. Sci. 605 (2011) 1048.
[21] Y.N. Xia, P.D. Yang, Y.G. Sun, Y.Y. Wu, B. Mayers, B. Gates, Y.D. Yin, F. Kim, H.Q. Yao, Adv. Mater. 15 (2003) 353.
[22] F. Cesano, S. Bertarione, M.J. Uddin, G. Agostini, D. Scarano, A. Zeccina, J. Phys. Chem. C 114 (2010) 169.
[23] M. Hodos, E. Horváth, H. Haspel, A. Kukovecz, Z. Kónya, I. Kiricsi, Chem. Phys. Lett. 399 (2004) 512.
[24] G.K. Mor, K. Shankar, M. Paulose, O.K. Varghese, C.A. Grimes, Nano Lett. 5 (2005) 191.
[25] S. Kubota, K. Johkura, K. Asanuma, Y. Okouchi, N. Ogiwara, K. Sasaki, T. Kasuga, J. Mater. Sci.: Mater. Med. 15 (2004) 1031.
[26] L. Kavan, M. Kalbac, M. Zukalova, I. Exnar, V. Lorenzen, R. Nesper, M. Graetzel, Chem. Mater. 16 (2004) 477.
[27] D.V. Baviykin, A.A. Lapkin, P.K. Plucinski, J.M. Friderich, F.C. Walsh, J. Phys. Chem. B 109 (2005) 19422.
[28] R. Huang, F. Chung, E.M. Kelder, J. Electrochem. Soc. 153 (2006) 459.
[29] S.S. Malwadkar, R.S. Gholap, S.V. Awante, P.V. Korake, M.G. Chaskar, N.M. Gupta, Photochem. Photobiol. A: Chem. 203 (2009) 24.
[30] V. Idakiev, Z. Yuan, T. Tabakova, B.-L. Su, Appl. Catal. A: Gen. 281 (2005) 149.
[31] T. Akita, M. Okumura, K. Tanaka, K. Ohkuma, M. Kohyama, T. Koyanagi, M. Date, S. Tsubota S, M. Haruta, Surf. Interface Anal. 37 (2005) 265.
[32] A. Erdőhelyi, J. Raskó, T. Kecskés, M. Tóth, M. Dömök, K. Baán, Catal. Today 116 (2006) 367.
[33] J. Raskó, M. Dömök, K. Baán, A. Erdőhelyi, Appl. Catal. A: Gen. 299 (2006) 202.
[34] M. Scott, M. Goeffroy, W. Chiu, M.A. Blackford, Top. Catal. 51 (2008) 13.
[35] M. Dömök, A. Oszkó, K. Baán, I. Sarusi, A. Erdőhelyi, Appl. Catal. A: Gen. 383 (2010) 33.
[36] R.M. Navarro, M.A. Peña, J.L.G. Fierro, Chem. Rev. 107 (2007) 3952.
[37] A. Gazsi, A. Koós, T. Bánsági, F. Solymosi, Catal. Today 160 (2011) 70.
[38] P.-Y. Sheng, G.A. Bowmaker, H. Idriss, Appl. Catal. A: Gen. 261 (2004) 171.
[39] M.A. Nadeem, M. Murdoch, G.I.N. Waterhouse, J.B. Metson, M.A. Keane, J. Llorca, H. Idriss, J. Photochem. Photobiol. A: Chem. 216 (2010) 250.
[40] Y. Guan, E.J.M. Hensen, Appl. Catal. A: Gen. 361 (2009) 49.
[41] M.J. Lippits, B.E. Nieuwenhuys, J. Catal. 274 (2010) 142.
[42] E. Horváth, Á. Kukovecz, Z. Kónya, I. Kiricsi, Chem. Mater. 19 (2007) 927.
[43] Á. Kukovecz, M. Hodos, E. Horváth, Gy. Radnóczi, Z. Kónya, I. Kiricsi, J. Phys. Chem. B 109 (2005) 17781.
[44] L.Z. Mezey, J. Giber, Jpn. J. Appl. Phys. 21 (1982) 1569.
[45] J. Kiss, K. Révész, F. Solymosi, Surf. Sci. 207 (1988) 36.
[46] L.K. Ono, B.R. Cuenya, J. Phys. Chem. C 112 (2008) 4676.
[47] F. Solymosi, M. Pásztor, J. Phys. Chem. 89 (1985) 4789.
[48] F. Gao, Y. Wang, D.W. Goodman, J. Phys. Chem. C 114 (2010) 4036.
[49] O. Ozturk, J.B. Park, S. Ma, J.S. Ratliff, J. Zhou, D.R. Mullins, D.A. Chen, Surf. Sci. 601 (2007) 3099.
[50] R. Ferrando, J. Jellinek, R.L. Johnston, Chem. Rev. 108 (2008) 845.
[51] A. Resta, J. Gustafson, R. Westerström, A. Mikkelsen, E. Lundgren, J.N. Andersen, M.M. Yang, X.F. Mab XF, X.H. Bao, W.X. Li, Surf. Sci. 602 (2008) 3057.
[52] J. Gong, B. Mullins, J. Am. Chem. Soc. 130 (2008) 16458.
[53] G.A.M. Hussein, N. Sheppard, M.I. Zaki, R.B. Fahim, J. Chem. Soc. Faraday Trans. 87 (1991) 2661.
[54] L. Óvári, F. Solymosi, Langmuir 18 (2002) 8829.
[55] J. Raskó, A. Hancz, A. Erdőhelyi, Appl. Catal. A: Gen. 269 (2004) 13.
[56] F. Solymosi, A. Erdőhelyi, M. Kocsis, J. Catal. 65 (1980) 428.